

Effect of Micro- and Nanoscale Topography on the Adhesion of Bacterial Cells to Solid Surfaces

Lillian C. Hsu,^a Jean Fang,^b Diana A. Borca-Tasciuc,^c Randy W. Worobo,^a Carmen I. Moraru^a

Department of Food Science, Cornell University, Ithaca, New York, USA^a; Department of Chemical Engineering, Massachusetts Institute of Technology, Cambridge, Massachusetts, USA^b; Department of Mechanical, Nuclear and Aerospace Engineering, Rensselaer Polytechnic Institute, Troy, New York, USA^c

Attachment and biofilm formation by bacterial pathogens on surfaces in natural, industrial, and hospital settings lead to infections and illnesses and even death. Minimizing bacterial attachment to surfaces using controlled topography could reduce the spreading of pathogens and, thus, the incidence of illnesses and subsequent human and financial losses. In this context, the attachment of key microorganisms, including *Escherichia coli*, *Listeria innocua*, and *Pseudomonas fluorescens*, to silica and alumina surfaces with micron and nanoscale topography was investigated. The results suggest that orientation of the attached cells occurs preferentially such as to maximize their contact area with the surface. Moreover, the bacterial cells exhibited different morphologies, including different number and size of cellular appendages, depending on the topographical details of the surface to which they attached. This suggests that bacteria may utilize different mechanisms of attachment in response to surface topography. These results are important for the design of novel microbe-repellant materials.

Attachment of bacteria to various surfaces often has adverse consequences. In dental offices and hospitals, adherent pathogenic bacteria may cause severe infections which hamper the recovery process and pose an extra threat to patients with already-weakened immune systems (1). In food processing facilities, the presence of spoilage or pathogenic microorganisms opens the possibility of transfer from food contact surfaces and processing equipment to the foods themselves. The consequences of such transfer events range from mild to severe illness resulting from consumption of contaminated foods to dramatic financial losses due to recalls and product losses (2). While planktonic cells usually can be effectively removed by physical means and/or killed by chemical sanitizers, they become much more difficult to remove when they form biofilms (3). Many food-borne pathogens, including *Escherichia coli* O157:H7, *Listeria monocytogenes*, *Bacillus cereus*, *Salmonella enterica* serovar Typhimurium, and *Campylobacter jejuni*, are known to form biofilms. Moreover, biofilms formed by these microorganisms may aid in trapping other harmful microbes that do not typically form biofilms, thereby allowing these species to survive and proliferate when they otherwise might not.

Among the many cellular and environmental factors affecting bacterial attachment and biofilm formation, surface roughness plays a very important role in this process. It is generally accepted that bacteria are more able to attach to crevices and pits where they are protected from unfavorable environmental disturbances (4). Surfaces with an R_a (arithmetic mean roughness) value of $\leq 0.8 \mu\text{m}$ are typically considered “hygienic,” whereas those with an R_a of $> 0.8 \mu\text{m}$ are more susceptible to bacterial deposition (5). Bacteria may attach to rougher surfaces in greater quantities for multiple reasons (6). Rougher surfaces offer higher surface area for attachment, while protecting the cells from shear forces. They may also foster local chemical changes to the surface properties; for example, surface conditioning by proteins may alter the surface charge, which may induce attractive electrostatic interactions with the bacteria. Additionally, surface irregularities make cleaning more difficult (7).

The role in bacterial attachment of surface roughness (i.e., the

presence of surface irregularities) at micrometric scale has been investigated by several groups. Boyd et al. (8) found that enhanced adhesion of *S. aureus* occurred on rougher stainless steel compared to its adhesion on smooth surfaces. Surfaces with features on the same scale as the *S. aureus* cells ($1 \mu\text{m}$) appeared to promote the strongest attachment due to maximal cell-substrate contact area. Whitehead et al. (9) also observed similar trends for bacterial species of different sizes. On the other hand, bacteria have been found to colonize smooth surfaces, such as electropolished stainless steel (10). Hence, surface roughness alone does not appear to be sufficient in predicting bacterial attachment, and surface topography needs to be considered next.

The effect of surface topography (i.e., the specific arrangement of the physical features on a surface) at the nanoscale on cellular attachment has been investigated far less. The biomedical field was the first to study extensively the response of the mammalian cells to topographic cues in the nanoscale range (11–14). Comparatively, only a few studies focus on bacteria. Although their response has been shown to be sensitive to nanoscale topographical details, no universal rules of attachment have been determined yet. Some researchers reported a greater level of attachment to nanophase surfaces (surfaces that have feature sizes smaller than 100 nm) than to conventional surfaces (4, 15, 16), while others found a bacterium-repellant effect of nanophase materials (17, 18). Park et al. (15) found that *Pseudomonas fluorescens* and *Pseudomonas putida* exhibited greater adhesion to nanophase titania than to nanometer-smooth topography, although the spatial distribution on the different surfaces was very similar.

All these studies suggest that bacteria respond differently to nanoscale topographical features and nanoscale-smooth topogra-

Received 7 November 2012 Accepted 6 February 2013

Published ahead of print 15 February 2013

Address correspondence to Carmen I. Moraru, cim24@cornell.edu.

Copyright © 2013, American Society for Microbiology. All Rights Reserved.

doi:10.1128/AEM.03436-12

phies, although no general rule emerges. This is not surprising, since bacterial attachment is a complex process which is not fully understood. Hence, the goal of this study is to further this knowledge by investigating the effect of feature size and periodicity on bacterial attachment. Silica and alumina surfaces, both of which have generally recognized as safe (GRAS) status and, thus, may be used in a wide range of biomedical and food applications, have been selected as substrate materials.

MATERIALS AND METHODS

Bacterial strains. Bacterial strains were selected based on their ability to form biofilms. Two nonpathogenic *Escherichia coli* strains, four *Pseudomonas fluorescens* strains, and seven pathogenic *E. coli* O157:H7 strains were screened using a rapid crystal violet assay slightly modified from the method of Cookson et al. (19). A single colony of each bacterial strain was inoculated into 2 ml tryptic soy broth (TSB) and incubated overnight at 30 and 37°C for *P. fluorescens* and *E. coli* strains, respectively, with shaking at 225 rpm. A 10- μ l loop of culture was inoculated into fresh tubes containing 2 ml TSB and grown statically for 48 h at 30 or 37°C for *P. fluorescens* and *E. coli* strains, respectively. After this growth period, the spent culture was removed from each test tube. Test tubes were rinsed three times with 3 ml sterile deionized water, inverted, and allowed to dry at 65°C for 30 min. Three ml of a 0.2% crystal violet solution was aliquoted into each test tube, incubated for 30 min at room temperature, and then removed. Test tubes were rinsed three times with 5 ml sterile deionized water and allowed to dry at room temperature overnight. Three ml of 95% ethanol was aliquoted into each test tube to elute the crystal violet. Absorbance readings were taken at 570 and 595 nm using a SpectraMax Plus 384 spectrophotometer (Molecular Devices, Sunnyvale, CA).

The results of the crystal violet assay led to the selection of *E. coli* ATCC 25922 and *P. fluorescens* as the nonpathogenic strains to use and *E. coli* O157:H7 as the pathogenic strain (data not shown). A nonpathogenic strain of *Listeria*, *Listeria innocua* FSL C2-008, was also used. The nonpathogenic strains of *E. coli* and *L. innocua* were obtained from the Food Safety Laboratory at Cornell University (Ithaca, NY). The pathogenic *E. coli* strains, as well as the *P. fluorescens* strains, were obtained from the collection of Randy Worobo (Cornell University, Geneva, NY).

Electrophoretic mobility. The electrophoretic mobility of bacterial cells was determined as an indication of their electric surface charge and was measured using a Malvern Zetasizer nano-ZS (Malvern Instruments Ltd., Malvern, Worcestershire, United Kingdom). Briefly, a 1:10 dilution of stationary-phase culture was made in TSB and gently vortexed to ensure thorough mixing. A 1-ml sample was aliquoted into the cuvette and inserted into the measurement chamber. Similarly, experiments were conducted to evaluate the electrophoretic mobility of the solid substrates. For this, small portions of each of the solid substrates were finely ground, and the fine powder was suspended in the same dilution fluid as the bacterial cells (TSB). The measurements were conducted in the same manner as for the bacterial cells. Measurements were taken in triplicate for each bacterial strain and solid substrate.

Hydrophobicity of bacterial cells. The hydrophobicity of bacterial cells was determined using the adhesion-to-hydrocarbon method described by Prachaiyo and McLandsborough (20). Briefly, bacterial cells from a stationary-phase culture were harvested by centrifugation at 9,000 rpm using a Hettich 32R benchtop centrifuge (Hettich Instruments, Beverly, MA). Cells were washed in 1 \times phosphate-buffered saline (PBS) and resuspended into 12 ml PBS. Four milliliters of bacterial suspension was aliquoted into each of three test tubes. One milliliter of xylene or hexadecane was added to each test tube. The third test tube contained only the cell suspension. Cells were then incubated for 10 min at 37°C, vortexed for 15 s, and incubated at 37°C for 30 min. The optical density of the cells after incubation with or without hexadecane or xylene at $\lambda = 540$ nm was measured, and the ratio of the optical density at 540 nm (OD_{540}) of the cells after incubation with hydrocarbon to that of the cells without hydrocarbon incubation was calculated and reported. These values represent

the percentage of cells that did not adhere to the hydrocarbons and remained in the aqueous phase. Cells are considered relatively hydrophobic when the values of the OD_{540} ratios are closer to 0 (indicating fewer cells remaining in aqueous phase) and relatively hydrophilic when the values are closer to 1 (20). Experiments were conducted in triplicate, and the values reported are average values with the standard deviation of three measurements.

Substrates. Topographically distinct silica dice and alumina membranes were used as substrates for bacterial attachment. For the silica substrates, commercially available silicon wafers were purchased from Silicon Quest International, Inc. (San Jose, CA). Three distinct nano- and microscale patterns of pores were created in 200-nm-thick thermally grown silicon dioxide in the Cornell Nanoscale Science and Technology Facility (Ithaca, NY). The features ranged in size from 500 to 1,500 nm and were defined by deep UV (DUV) lithography using an ASML PAS5500/300C DUV stepper (ASML, Veldhoven, Netherlands). Subsequent dry etching was used to create wells with a depth of 27 to 32 nm. Well depth was confirmed using a Veeco 6 M profilometer (Veeco, Plainview, NY), and the surface features' size and shape were verified by scanning electron microscopy (SEM) using a Zeiss LEO 1550 FE-SEM (Zeiss, Oberkochen, Germany) in the Cornell University Center for Materials Research (Ithaca, NY). Alumina membranes with pores of 20 or 200 nm (Anodisc 6809-6002 and 6809-6022) were purchased from Whatman (GE Healthcare, United Kingdom), and nanosmooth alumina substrates were purchased from Alfa Aesar (Ward Hill, MA).

Contact angle measurements. The hydrophobicity of the solid surfaces was evaluated by performing contact angle measurements by the sessile drop method using a Rame-Hart 500 goniometer (Rame-Hart, Inc., Succasunna, NJ). Briefly, 15- μ l droplets of water were allowed to contact the surface of each substrate, and advancing and receding angles were measured. Reported values are the averages of the advancing and receding angles. All measurements were performed in triplicate.

Surface roughness. Surface roughness characterization was performed by atomic force microscopy (AFM) using Veeco DI-3100 (Veeco, Plainview, NY) and PicoPlus (Molecular Imaging, Tempe, AZ) microscopes. The average roughness (R_a), root-mean-square roughness (R_{rms}), and 10-point height (R_z) were extracted from the AFM images by using the free and open source software Gwyddion (<http://gwyddion.net/>).

Attachment and biofilm studies. A single colony of each bacterial strain was streaked onto tryptic soy agar (TSA) plates and incubated at the appropriate temperature overnight. The following day, a single colony was inoculated into test tubes containing TSB and grown overnight at 30°C for *P. fluorescens* or 37°C for *E. coli* and *L. innocua* strains, with shaking at 225 rpm. A loop of culture was transferred into a fresh tube of TSB and incubated with shaking until stationary phase was reached (12 to 18 h). The stationary-phase culture contained approximately 10^7 to 10^8 CFU/ml.

Alumina membranes were rinsed with 100% ethanol and air dried in a laminar flow hood prior to use. Nanosmooth alumina substrates and silica surfaces were rinsed with 100% ethanol and autoclaved in sterilizing pouches (ThermoFisher Scientific, Pittsburgh, PA) for 15 min at 121°C prior to use. Substrates with micro- and nanoscale topography were not reused, but the nanosmooth alumina substrates were cleaned and reused after visualization of attached cells by fluorescence microscopy. Immediately after fluorescence imaging was completed, the substrates were sonicated for 30 min in a heated solution of Alconox and water. After rinsing with deionized water, the substrates were again sonicated in 95% ethanol for 30 min. Substrates were then rinsed, air dried, and autoclaved prior to reuse. Substrates that were reused were periodically visualized using SEM (without sputter coating) to confirm that surface details were not altered and that the cleaning regimen was able to remove all organic matter.

For the experiments with alumina substrates, one of each type of substrate (porous 20-nm and 200-nm membranes and nanosmooth substrate) was placed into a 60- by 15-mm petri dish (VWR International) containing 5 ml of culture. For the silica substrate, a single dice containing

the three designed topographies and the nanosmooth control surface was inserted into a test tube containing stationary-phase bacterial cells. All substrates were incubated for 30 min or 24 h for bacterial attachment analysis or 96 h for observation of biofilm development. Experiments were conducted in duplicate.

Fluorescence microscopy. A wide-field fluorescence Olympus BX-51 microscope (Olympus, Center Valley, PA) equipped with a Roper Cool-Snap HX charge-coupled-device (CCD) camera (Roper Scientific, Ottobrunn, Germany) was used for epifluorescent imaging of cells stained with the LIVE/DEAD dyes (Molecular Probes, Invitrogen). Substrates with attached bacteria were removed from the cell culture with tweezers, gently rinsed three times with sterile deionized water to remove any loosely adherent cells and excess medium, and placed in new petri dishes. Equal parts of SYTO 9 and propidium iodide nucleic acid stains were mixed with sterile deionized water, and the solution was aliquoted into the petri dishes according to the manufacturer's protocol. Substrates were incubated with the fluorescent dyes in the dark for at least 15 min prior to visualization. Each substrate was visualized under a 100 \times oil immersion lens, and 10 fields of view were randomly chosen for analysis. Images were processed using Fireworks (Adobe), and cell counts were obtained using ImageJ (NIH, <http://rsbweb.nih.gov/ij/>).

Scanning electron microscopy. Bare substrates were visualized without surface coating, using a Zeiss LEO 1550 FE-SEM (Zeiss, Oberkochen, Germany). Substrates exposed to bacterial cells were immersed in nitrogen slush for 10 s, freeze-dried using a Labconco FreeZone freeze dryer (Labconco Corp., Kansas City, MO) for 24 h, and then mounted onto stubs. Carbon was evaporated onto the freeze-dried surfaces prior to visualization.

Images obtained by SEM were visually analyzed to determine the size and number of bacterial appendages that were visible on the attached cells. The number of appendages was categorized into the following groups: 0 to 5, 6 to 10, 11 to 15, 16 to 25, and ≥ 25 . Cells categorized as ≥ 25 had too many appendages to count.

Statistical analysis. Statistical analysis was performed using Microsoft Excel (Microsoft Corp., Redmond, WA) and JMP 9 (SAS, Cary, NC). The *t* test was used to evaluate statistical differences in cell hydrophobicity. The statistical differences for the numbers of cells adhered to the various surfaces were evaluated using multivariate analysis of variance (MANOVA), with surface topography as a fixed variable and the effect of the replicate as a random variable. A similar procedure was used for analyzing differences in cell morphology. Differences were considered statistically significant at a *P* value of < 0.05 .

RESULTS

Bacterial surface properties. The electrophoretic mobility of the bacterial strains used in this study was used as an indicator of the electrical charge of the cell surface. All strains had a negative surface charge, as the electrophoretic mobilities of *E. coli* ATCC 25922, *E. coli* O157:H7 4477, *L. innocua*, and *P. fluorescens* 1150 cells in stationary phase were -0.87 ± 0.11 (average \pm standard deviation), -0.74 ± 0.02 , -1.37 ± 0.06 , and $-0.24 \pm 0.02 \mu\text{s}^{-1}/(\text{V}/\text{cm})$, respectively (Table 1).

Another property of the bacterial cells known to play an important role in attachment is their surface hydrophobicity. It has been shown before that bacterial strains with similar hydrophobic properties show similar adhesion patterns to surfaces and that hydrophobic surfaces favor adhesion of hydrophobic bacteria (21). The relative hydrophobicity of the bacterial strains used in this work was measured using their adhesion to both hexadecane and xylene, since the results of hydrocarbon attachment measurements may vary depending on the hydrocarbons tested (20). In this study, the attachment results were similar for hexadecane and xylene, as shown by the data in Table 1. The relative hydrophobicity measurements indicated that the *E. coli* strains were least hy-

TABLE 1 Hydrophobicity and electrophoretic mobility of bacterial strains

Bacterial strain	Hydrophobicity on ^a :		Avg electrophoretic mobility [$\mu\text{s}^{-1}/(\text{V}/\text{cm})$] \pm SD ^b
	Hexadecane	Xylene	
<i>E. coli</i> ATCC 25922	0.92 \pm 0.06	0.92 \pm 0.00 AC	-0.87 ± 0.11
<i>E. coli</i> O157:H7 4477	0.96 \pm 0.01 AB	0.87 \pm 0.02 BD	-0.74 ± 0.02
<i>L. innocua</i> FSL C2-008	0.81 \pm 0.06 A	0.71 \pm 0.03 AB	-1.37 ± 0.06
<i>P. fluorescens</i> 1150	0.84 \pm 0.03 B	0.61 \pm 0.09 CD	-0.24 ± 0.02

^a Hydrophobicity was determined as bacterial adhesion to hydrocarbons. Statistically significant differences are denoted by subscript letters, where the same subscript indicates a significant difference between two values.

^b Electrophoretic mobility was measured in tryptic soy broth (pH 7.18).

drophobic, followed by *L. innocua* and *P. fluorescens*, which was the most hydrophobic. The differences in relative hydrophobicity in hexadecane were statistically significant between *E. coli* O157:H7 and *L. innocua* and, also, between *E. coli* O157:H7 and *P. fluorescens*. In xylene, the relative hydrophobicity was statistically different only between *L. innocua* and the two *E. coli* strains and between *P. fluorescens* and the *E. coli* strains.

Substrate properties. (i) Surface charge. The substrate surfaces were made out of negatively charged materials, in order to maximize electrostatic repulsion between the surfaces and the negatively charged bacteria. Alumina and silica have both been reported to be negatively charged at the pH used in this study (pH 7.3) (22, 23). This was confirmed by the data in Table 2.

(ii) Surface topography. The dimensions of the topographical details for the silica substrates were designed taking into consideration the size and shape of the bacterial cells. Four distinct topographies were designed and fabricated on the silica substrates: circular wells with a diameter of 500 nm and interwell spacing of 200 nm (Fig. 1a), narrow rounded rectangular wells with dimensions of 1 by 1.5 μm and interwell spacing of 2 μm (Fig. 1b), wide rounded rectangular wells with dimensions of 1 by 2 μm and interwell spacing of 500 nm (Fig. 1c), and a nanosmooth surface used as a control (not shown). All the wells were 27 to 32 nm deep. Alumina (ceramic) membranes with nominal pore diameters of 20 and 200 nm, respectively, were used as substrates with topographic details in the nanometric range, much smaller than the size of the bacterial cells.

(iii) Surface roughness. As seen in Table 2, all nonporous surfaces used in this study had roughness values in the hygienic range ($R_a < 0.8 \mu\text{m}$) (5). These values indicate that the surface features of these surfaces would not allow bacteria to penetrate into the surface, but merely sit on the surface details. Although roughness values could not be determined accurately for the porous alumina membranes, the pore diameters would not permit cells to penetrate into those surfaces either.

(iv) Surface hydrophobicity. It is generally accepted that contact angles greater than 90 $^\circ$ denote hydrophobic surfaces, while contact angles smaller than 45 $^\circ$ denote clearly hydrophilic surfaces (10). Contact angle measurements confirmed that all surfaces were hydrophobic (Table 2). Smooth silica had a contact angle of 89 $^\circ$, whereas smooth alumina had a contact angle of 83 $^\circ$. The patterned silica surfaces were slightly more hydrophobic than the smooth silica, with contact angles ranging between 94 and 98 $^\circ$. The nanosmooth alumina substrate was slightly less hydrophobic than the silica wafers. It was not possible to accurately measure the contact angles of the alumina membranes, due to their porosity,

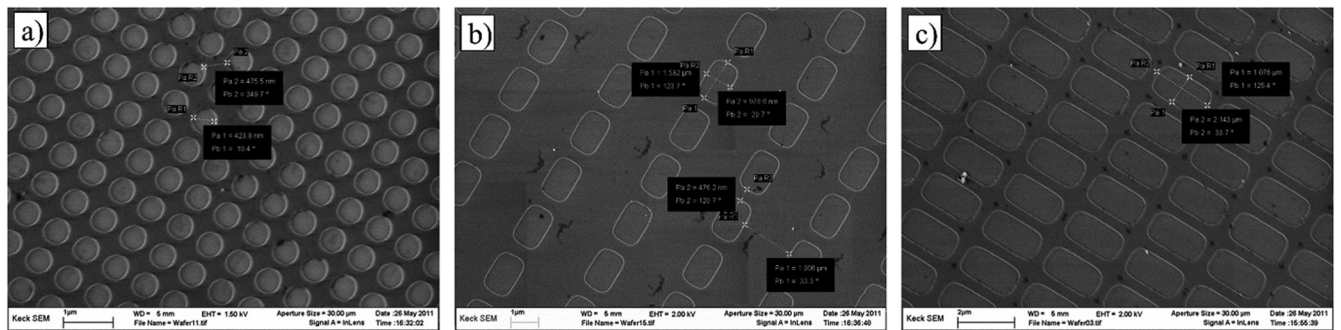


FIG 1 Scanning electron micrographs of individual sections of the engineered silica substrates. (a) Circular wells; (b) thin wells; (c) wide wells.

but based on the contact angle of the smooth alumina, they were also assumed to be hydrophobic.

Bacterial attachment to the substrate surfaces. The attachment to the various surfaces was evaluated from two different perspectives: the existence of a pattern of attachment (qualitative attachment) and the total number of bacteria attached for each surface (quantitative attachment).

Qualitative evaluation of attachment. Some interesting attachment patterns were noticed on the silica substrates. The cells appeared to attach more onto the smooth areas of the surface between the wells, rather than inside the wells. This can be observed in Fig. 2, which shows examples of cells (both live and dead) of *E. coli* ATCC 25922, *L. innocua*, and *P. fluorescens* attached to the silica surfaces with rectangular wells at the 30-min time point. These attachment patterns suggest that cells responded to the surface topography by maximizing the contact area between the cell and the surface. After 96 h, the patterns vanished: microcolonies and emerging biofilms were observed; however, the multilayered bacterial cells did not exhibit any specific orientation. No particular trends of attachment were observed on the alumina nanoporous membranes, even at the 30-min time point. This is not surprising, since the features on those substrates (circular pores) were distributed in an isotropic fashion. Orientation was also random on both types of nanosmooth surfaces.

Quantitative evaluation of bacterial attachment. The fluorescent images were analyzed to yield insight into the total number of

strongly attached cells at various time points. The relative proportions of live and dead cells present on the surfaces were also assessed. As shown in Fig. 3, while the attachment was similar for different bacterial strains on the nanoporous ceramic membranes, a trend emerges for the nanosmooth alumina and the silica substrates. For silica substrates, the order of attachment was *E. coli* ATCC 25922 > *L. innocua* ~ *P. fluorescens* > *E. coli* O157:H7.

Figures 4 and 5 show the average numbers of live, dead, and total cells attached to each type of substrate for different time points: 30 min, 24 h, and 96 h. The stacked bar graphs allow an overall assessment of differences in attachment trends with time, which are described next.

Attachment to the alumina membranes. The attachment trends observed for the alumina substrates (Fig. 4) were species specific. At the 30-min time point, all three Gram-negative bacteria exhibited greater attachment on the nanoporous

TABLE 2 Physical properties of the solid substrates

Substrate	Roughness parameters (nm ^a)			Avg contact angle (°) ± SD	Avg electrophoretic mobility [$\mu\text{s}^{-1}/(\text{V}/\text{cm})$] ± SD ^b
	R _a	R _{rms}	R _z		
Alumina					
Nanosmooth	4.9	6.3	27	83 ± 2	-1.24 ± 0.22
Porous (20 nm and 200 nm)	NA ^c	NA	NA	NA	-0.29 ± 0.09
Silica					
Nanosmooth	0.3	0.3	1.6	89 ± 2	-0.04 ± 0.04
Circular wells	6.7	7.5	26.7	98 ± 8	
Thin rectangular wells	6.4	7.3	23.3	94 ± 7	
Wide rectangular wells	5.2	6.1	19.3	95 ± 7	

^a One nanometer is 10⁻⁹ m.

^b Electrophoretic mobility was measured in tryptic soy broth (pH 7.18).

^c NA, not applicable; roughness and contact angle could not be determined accurately for the porous surfaces.

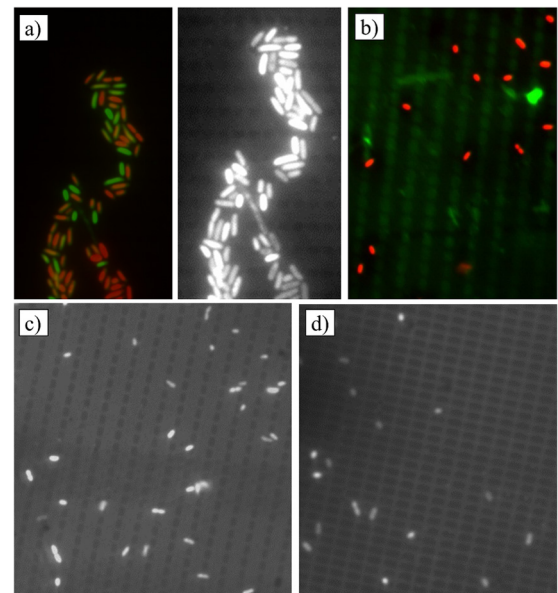


FIG 2 Fluorescence microscopic images of attached cells after 30 min, showing preferential positioning relative to surface topography. (a) *E. coli* ATCC 25922 on silica with thin wells (photos are two versions of the same field; the black and white image accentuates the topographical details). (b) *L. innocua* on silica with thin wells. (c to d) *P. fluorescens* on thin-well silica and wide-well silica, respectively. In the color images, dead cells are shown in red, live cells are shown in green.

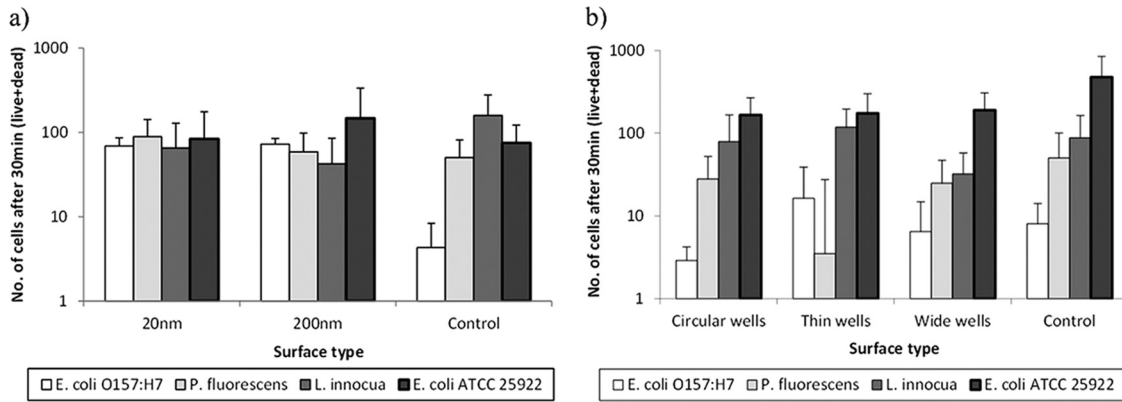


FIG 3 Average numbers of total bacterial cells attached after 30 min on alumina (a) and silica (b). Error bars show one standard deviation.

membranes than on the control ($P < 0.05$). However, the Gram-positive *L. innocua* showed the opposite trend, with the greatest amount of cellular attachment being observed on the control surfaces, although only the difference between the 200-nm membranes and the control surface was significantly different ($P < 0.05$). After 24 h, no statistically significant differences between the attachment of *E. coli* ATCC 25922 and

pathogenic *E. coli* onto the various surfaces were observed. *P. fluorescens* showed preferential attachment to the 200-nm membranes and very sparse attachment to the 20-nm membranes. *L. innocua* also showed significantly greater attachment to the 200 nm-membrane than to the controls ($P < 0.05$). After 96 h, less attachment of *E. coli* ATCC 25922 was observed on the 200-nm nanoporous membranes than on controls ($P < 0.05$).

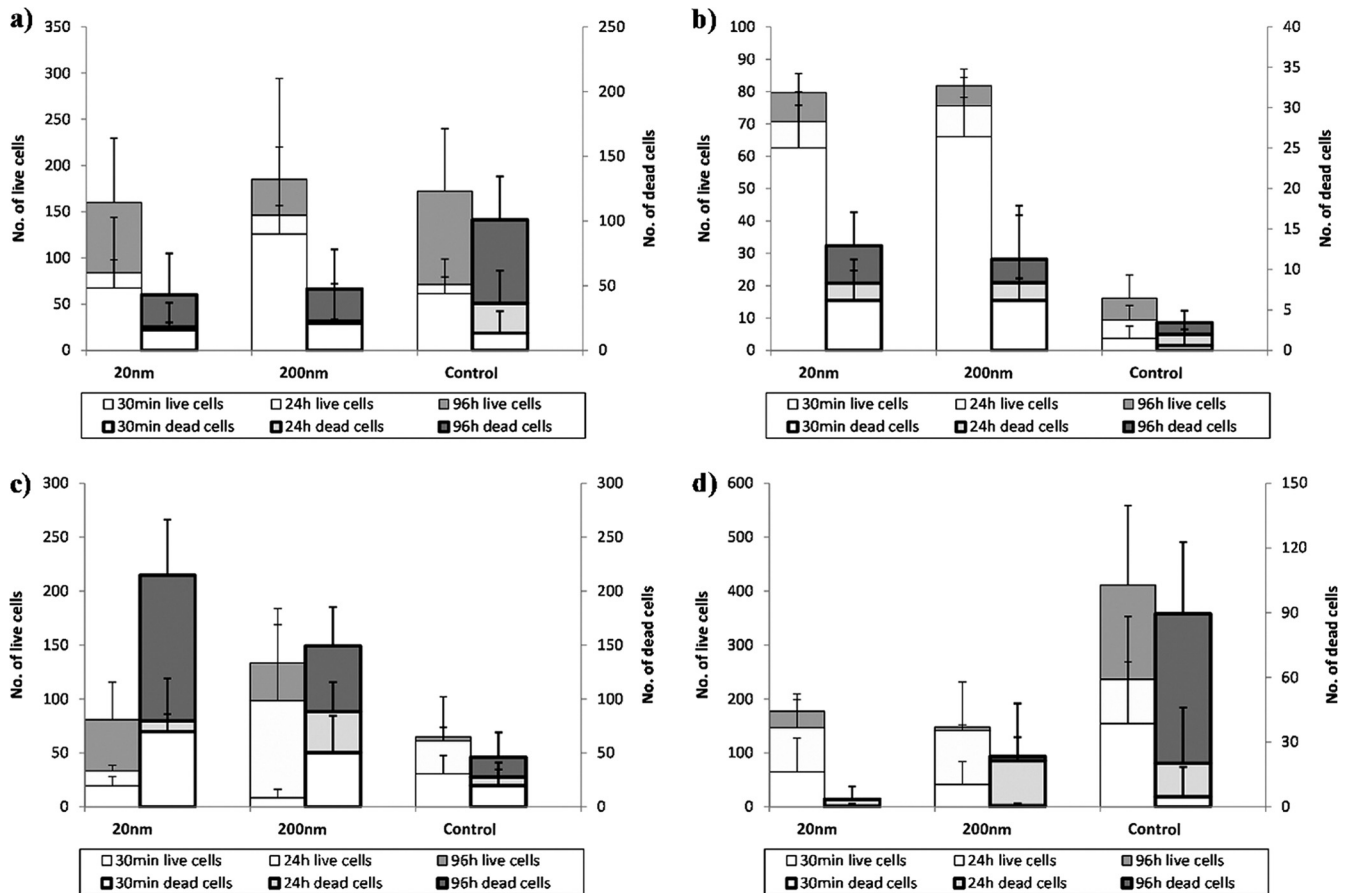


FIG 4 Average numbers of live (thin borders, left axis) and dead (thick borders, right axis) cells attached after 30 min, 24 h, and 96 h on alumina surfaces. (a) *E. coli* ATCC 25922; (b) *E. coli* O157:H7 4477; (c) *P. fluorescens* 1150; (d) *L. innocua* FSL C2-008. The units on the y axes represent number of cells per microscopic field (for additional details, refer to Materials and Methods). Error bars show standard deviations.

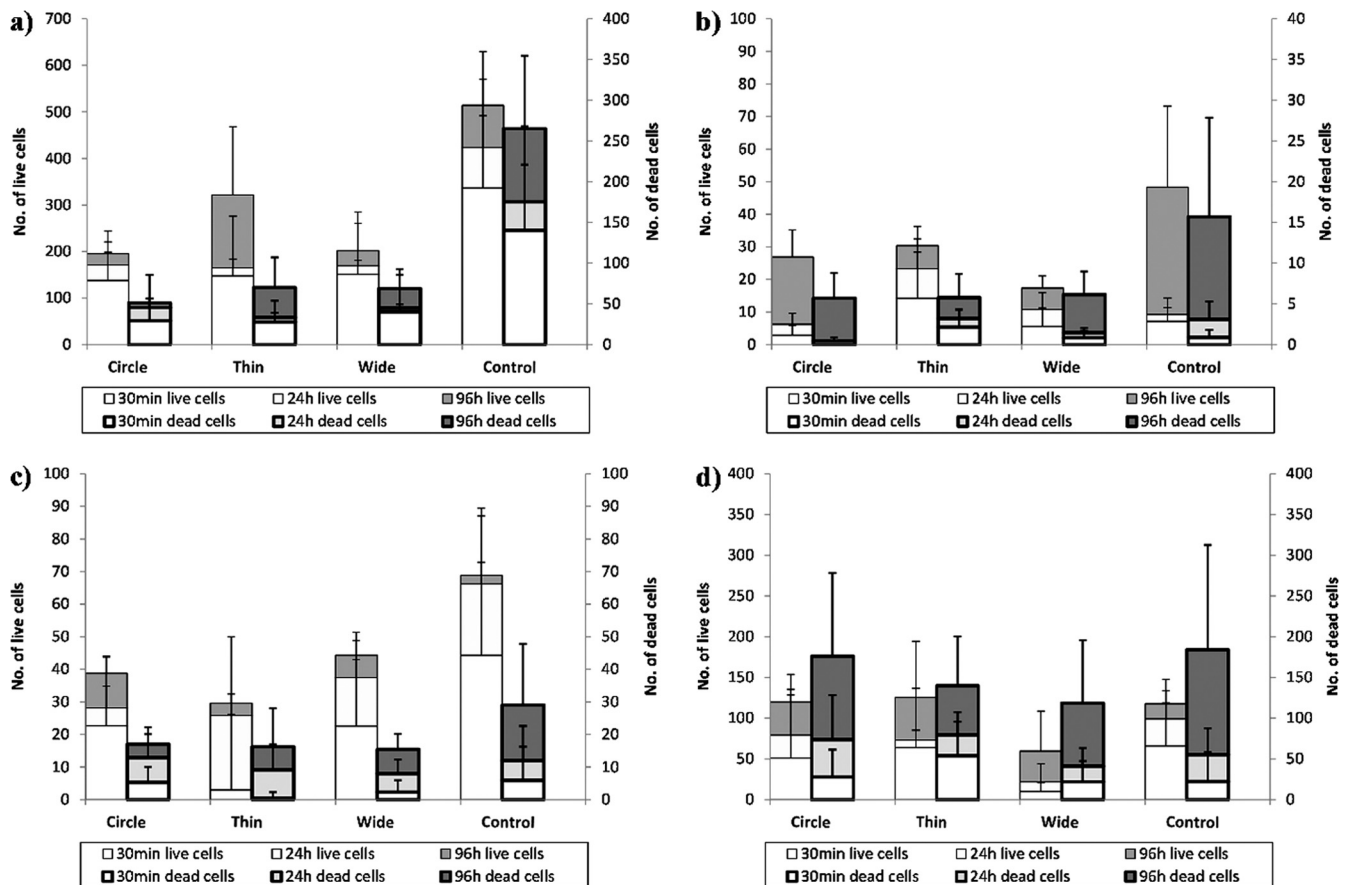


FIG 5 Average numbers of live (thin borders, left axis) and dead (thick borders, right axis) cells attached after 30 min, 24 h, and 96 h on silica surfaces. (a) *E. coli* ATCC 25922; (b) *E. coli* O157:H7 4477; (c) *P. fluorescens* 1150; (d) *L. innocua* FSL C2-008. The units on the *y* axis represent number of cells per microscopic field (see description in Materials and Methods). Error bars show standard deviations.

For *L. innocua*, attachment to both nanoporous membranes was less than to the control. Both the pathogenic *E. coli* and *P. fluorescens* had greater levels of attachment to the nanoporous membranes than to controls, though only *P. fluorescens* attachment to the 20-nm membranes was statistically different than its attachment to the control.

To summarize, for most time points, *E. coli* ATCC 25922 and *L. innocua* showed more attachment on the nanosmooth control than on the 20-nm- and 200-nm-pore-size membranes; these differences were most pronounced at 96 h, the time point at which a mature biofilm was formed. *E. coli* O157:H7 and *P. fluorescens* showed the opposite trend, with the least attachment on the control for most time points. These trends were consistent between the live and dead cells but more pronounced for the live cells.

Attachment to the silica surfaces. For the two *E. coli* strains and *P. fluorescens*, bacterial cells consistently exhibited higher levels of attachment to the nanosmooth silica control surfaces than to the patterned surfaces, overall and for most time points (Fig. 5). For all three microorganisms, these differences were most pronounced at 96 h, in the mature biofilm stage. For the Gram-positive *L. innocua*, although the same preferential attachment to the smooth areas of the patterned surfaces as for the other three microorganisms was observed in the microscopic images, there were no statistically significant differences ($P < 0.05$) in the numbers of

attached cells among the different silica surfaces at the different time points.

Cell morphology of attached bacteria. In order to observe whether or not exposure to the different surfaces induced morphological differences in the attached cells, a visualization of the attached bacteria by SEM was conducted. For this, the 24-h time point was chosen in order to have a sufficient number of attached cells remaining after sample preparation, but not so many cells as to obscure the initial layer of attached cells. The morphology of *E. coli* O157:H7 was not examined.

Cell size. First of all, some significant differences in cell size were observed for the cells attached to the porous alumina substrates and those attached to the smooth controls. *L. innocua* cells attached to the 20-nm and 200-nm membranes were significantly larger than the cells on the control surfaces; *E. coli* ATCC 25922 and *P. fluorescens* cells attached to the 200-nm membrane were also larger than cells of these organisms on the control or the 20-nm membrane (Table 3). For the silica substrates, although cells attached to the patterned surfaces were slightly smaller than those on the controls, the observed differences were not statistically significant (Table 4).

Cellular appendages. SEM visualization of attached bacteria revealed striking physical differences between cells attached to different surface types, especially for *E. coli* ATCC 25922 and *P. fluo-*

TABLE 3 Cell and appendage dimensions for microorganisms attached on alumina substrates

Microorganism and morphological feature	Avg dimension (μm) \pm SD on surface with indicated roughness ^a		
	Control	20 nm	200 nm
<i>E. coli</i> ATCC 25922			
Cell diam	0.58 \pm 0.16	0.78 \pm 0.07*	0.63 \pm 0.21
Cell length	2.10 \pm 0.44	1.99 \pm 0.24	2.60 \pm 0.72*
Appendage diam	0.070 \pm 0.01	0.05 \pm 0.030	0.04 \pm 0.01
Appendage length	0.99 \pm 0.52	1.09 \pm 0.80	1.66 \pm 1.18
<i>L. innocua</i>			
Cell diam	0.42 \pm 0.04	0.530 \pm 0.05*	0.49 \pm 0.05
Cell length	1.11 \pm 0.07	1.36 \pm 0.25*	1.16 \pm 0.20
<i>P. fluorescens</i>			
Cell diam	0.53 \pm 0.11	0.76 \pm 0.14	0.87 \pm 0.09*
Cell length	1.86 \pm 0.45	2.29 \pm 0.45	2.41 \pm 0.60
Appendage diam	0.10 \pm 0.02	0.06 \pm 0.02	0.06 \pm 0.03
Appendage length	0.89 \pm 0.95	1.31 \pm 0.55	1.19 \pm 0.44

^a One micrometer is 10^{-6} m. *, value is significantly different from that of the control.

rescens 1150 (Fig. 6 and 7). Both *E. coli* ATCC 25922 and *P. fluorescens* 1150 cells expressed appendages that likely assisted in their attachment to the surfaces. Virtually no appendages were observed for *L. innocua* cells. For the strains that expressed appendages, the types of appendages that were present appeared to depend on the surface topography of the substrate.

E. coli ATCC 25922 cells exhibited long and relatively thick appendages that were few in number on both the nanosmooth alumina and on all silica surfaces. On the 20-nm porous alumina membranes, a much more complex web of appendages was seen linking cells to each other, as well as to the surface (Fig. 6, middle). On the 200-nm porous membranes, the cells expressed more numerous but thinner appendages that formed thick bundle structures (Fig. 6, bottom). On all silica surfaces, the *E. coli* ATCC 25922 cells expressed shorter and thinner appendages that often extended into the wells, even if the cells themselves were not located inside the wells (Fig. 7).

P. fluorescens expressed shorter appendages than *E. coli* ATCC 25922, especially on the smooth silica (Tables 3 and 4). On both the 20-nm and 200-nm porous alumina membranes, thick appendages surrounded the cells and formed dense webs that connected cells to each other and to the surface (Fig. 6). On the engineered wide-welled or narrow-welled silica substrates, *P. fluorescens* cells expressed long appendages similar to those seen on the smooth silica surfaces (Fig. 6 and 7). Cells attached to the silica surfaces featuring circular wells appeared to express few to no appendages, which were shorter than those seen on the other silica substrates. Moreover, the dense, weblike network observed on the alumina membranes was not seen on any of the silica surfaces.

Quantification of the number of appendages for the attached cells revealed an interesting trend. As shown in the cumulative frequency graphs in Fig. 8, for both *E. coli* and *P. fluorescens*, the cells attached to the nanoporous membranes expressed many more appendages than the cells attached to nanosmooth alumina. No obvious trends in the number of expressed appendages were observed for the cells attached to silica surfaces, except for the fact that the cells attached to the wide-well surfaces seemed to have

TABLE 4 Cell and appendage dimensions for microorganisms attached on silica substrates

Microorganism and morphological feature	Avg dimension (μm) \pm SD on surface with indicated topography ^a			
	Control	Circular wells	Thin wells	Wide wells
<i>E. coli</i> ATCC 25922				
Cell diam	0.63 \pm 0.04	0.54 \pm 0.07*	0.62 \pm 0.09	0.59 \pm 0.04
Cell length	2.22 \pm 0.29	2.12 \pm 0.62	2.31 \pm 0.54	2.48 \pm 0.25
Appendage diam	0.07 \pm 0.01	0.07 \pm 0.02	0.07 \pm 0.01	0.06 \pm 0.02
Appendage length	1.48 \pm 0.56	0.56 \pm 0.37	0.58 \pm 0.46	1.62 \pm 1.22
<i>L. innocua</i>				
Cell diam	0.52 \pm 0.03	0.44 \pm 0.07	0.45 \pm 0.03	0.50 \pm 0.03
Cell length	1.26 \pm 0.15	1.25 \pm 0.12	1.14 \pm 0.15	1.30 \pm 0.19
<i>P. fluorescens</i>				
Cell diam	0.60 \pm 0.09	0.57 \pm 0.07	0.52 \pm 0.06	0.49 \pm 0.07
Cell length	1.84 \pm 0.51	2.48 \pm 0.46	1.67 \pm 0.29	1.54 \pm 0.43
Appendage diam	0.10 \pm 0.12	0.03 \pm 0.01*	0.10 \pm 0.02	0.10 \pm 0.01
Appendage length	0.82 \pm 0.32	0.33 \pm 0.12*	1.79 \pm 0.89	1.49 \pm 0.82

^a One micrometer is 10^{-6} m. *, value is significantly different from that of the control.

slightly fewer appendages per cell than did cells attached to the other silica surfaces.

DISCUSSION

The results of this study clearly demonstrate that substrate topography at the micro- and nanoscale does influence bacterial attachment behavior, both in terms of the orientation of the cells relative to the surface details and the number of cells attached to a particular surface. It is clear that bacterial attachment is influenced by the shape and size of the topographical features, as evidenced by the preferential orientation that cells exhibited on the silica surfaces. Cells aligned themselves in ways that would maximize contact area between the cell and the surface. This preferential alignment to micro- and nanoscale surface details has been observed by others as well. Díaz et al. (24) found that *P. fluorescens* attached in the channels of nanostructured gold. Hochbaum and Aizenberg (25) found that *P. aeruginosa* cells aligned themselves horizontally in trenches when the vertical nanoposts were spaced far enough apart to accommodate the cells; however, when the interpost spacing was smaller than the diameter of the cells, bacteria aligned themselves parallel to the vertical posts and perpendicular to the plane of the substrate surface.

The fact that no universal relationship between the surface topography and the number of attached cells was observed and the fact that the number of attached cells varied with each strain are not unexpected results, as the outer membrane of bacteria can be vastly different between species. Apparently conflicting results have been reported in the literature as well, with some researchers finding a greater level of attachment to nanophase surfaces than to conventional surfaces (4, 15, 16), while others found a bacterium-repellant effect of nanophase materials (18). Work conducted by Singh et al. (26) on titania thin films suggests a relationship between surface roughness and bacterial attachment: as roughness increased to approximately 20 nm, bacterial attachment increased as well; above 20 nm, significant inhibition of bacterial attachment and biofilm formation were observed.

Perhaps the most compelling evidence of a substrate topogra-

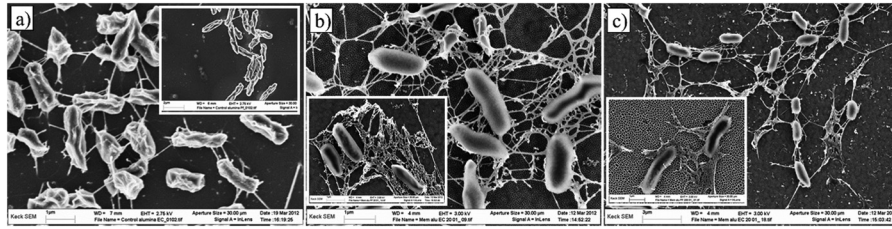


FIG 6 Scanning electron micrographs of *E. coli* ATCC 25922 (large photos) and *P. fluorescens* (insets) cells attached to alumina substrates after 24 h. (a) Nanosmooth control; (b) 20-nm membrane; (c) 200-nm membrane.

phy effect on bacterial attachment is the observation that the attached cells showed differences in their size and morphology, which varied with the surface and surface topography. Overall, bacteria attached to the nonporous surfaces, i.e., the nanoengineered silica substrates and the smooth alumina and silica control substrates, exhibited fewer individual appendages than cells attached to the nanoporous membranes. Additionally, the appendages were thicker for cells attached to the nonporous substrates than for those present on the porous substrates. In a study by Rizzello et al. (27), *E. coli* cells exposed to gold substrates with nanoscale topography did not express certain type-1 fimbriae, in contrast to cells exposed to smooth gold and glass surfaces. A comprehensive analysis of the *E. coli* proteome showed that, in addition to fimbria expression, genes involved in stress response and defense mechanisms were expressed differently in cells exposed to nanorough and nanosmooth surfaces.

While it is not possible to definitively identify the types of appendages expressed by *E. coli* ATCC 25922 and *P. fluorescens* on the different surfaces based on the SEM images alone, visual observations strongly suggest that the appendages are not the same. Quantitative analysis of the numbers of appendages protruding

from the attached cells further supports the conclusion that substrate surface topography is affecting attachment. In particular, cells attached to nanoporous membranes had many more appendages than those attached to nanosmooth alumina. These appendages resemble fimbriae, which have a known role in attachment, while the few short appendages for cells attached to silica substrates resemble conjugation pili (28, 29). Whether or not the size and morphological changes observed in this study play a role in attachment or represent a different, unrelated reaction to the nanophase surfaces is at this point unclear. Further investigations are needed to positively identify the type of appendages expressed by the cells attached to different surfaces used in the current study and elucidate their role in attachment, as well as the other mechanisms that the cells employ to attach to surfaces with micro- and nanoscale topography.

Overall, the results of this work clearly show that substrate surface topography at the micro- and nanoscale affects bacterial attachment. Cells seem to try to maximize contact area with the surfaces, presumably to achieve a stronger and more stable attachment, which results in a specific alignment of the cells depending on the arrangement of the topographical details. Moreover, sur-

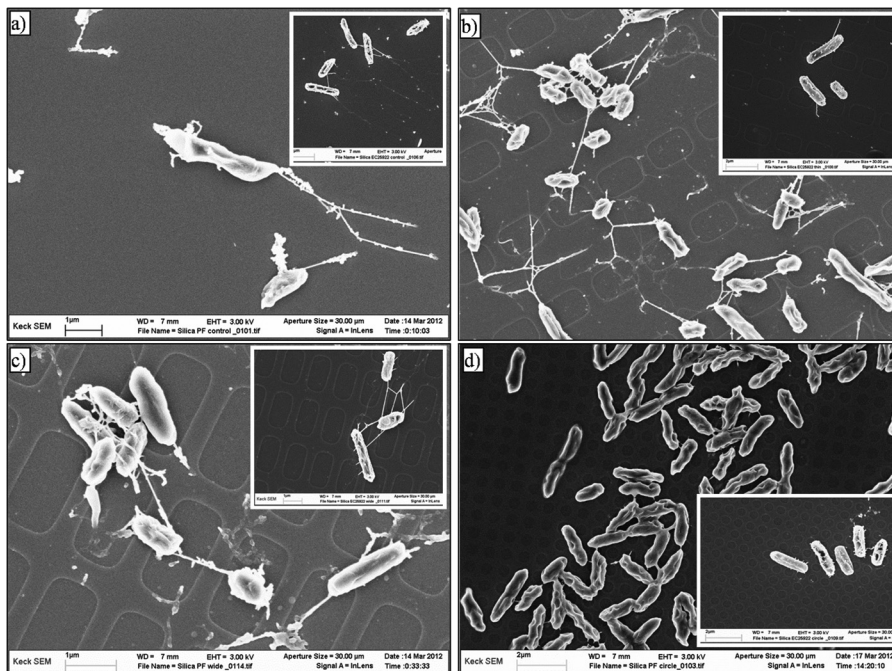


FIG 7 Scanning electron micrographs of *E. coli* ATCC 25922 (large photos) and *P. fluorescens* (insets) cells attached to silica substrates after 24 h. (a) Nanosmooth control; (b) thin wells; (c) wide wells; (d) circular wells.

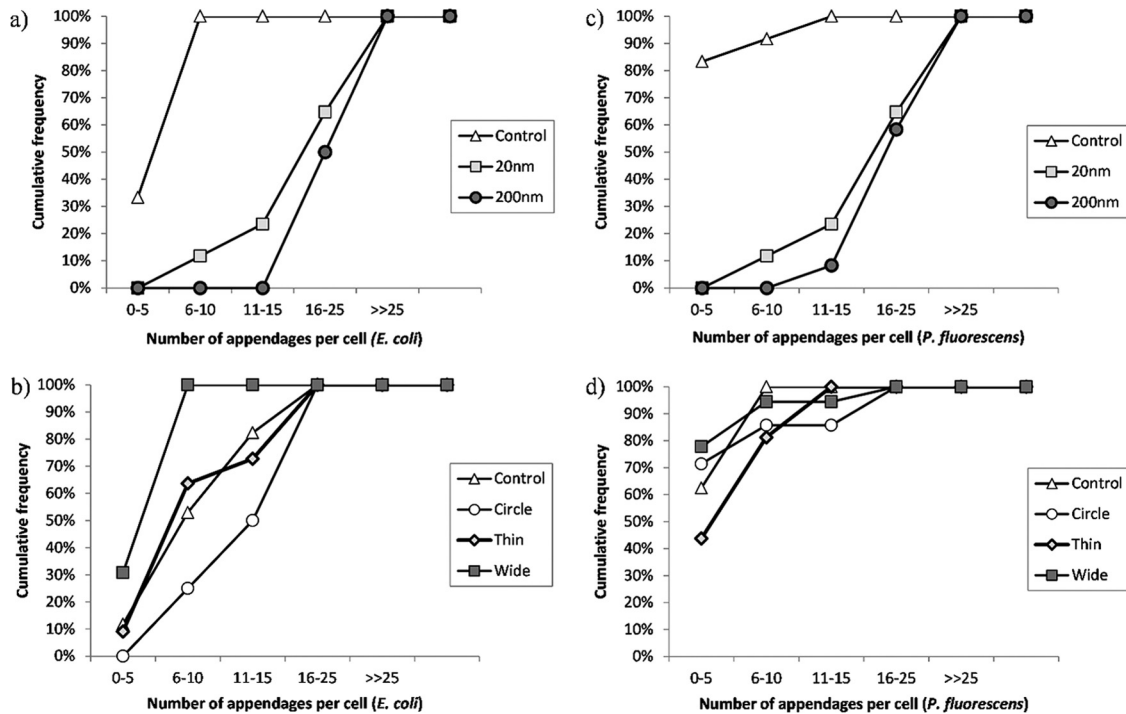


FIG 8 Numbers of appendages per cell (at 24 h) for *E. coli* ATCC 25922 cells attached to alumina substrates (a) and silica substrates (b) and *P. fluorescens* cells attached to alumina substrates (c) and silica substrates (d).

face topography appears to induce the expression of different types of appendages that might mediate attachment. Better understanding of the way in which bacterial cells attach to surfaces with controlled topography in the micro- and nanoscale will allow the design and fabrication of materials able to effectively control bacterial adhesion, with a large number of potential biomedical and industrial applications.

ACKNOWLEDGMENTS

Funding for this project was provided by USDA-NIFA project 65210-20024-11 and USDA National Needs grant no. 2006-04257.

The fabrication of silica surfaces was performed by Joshua Phelps. His assistance with this project is acknowledged and tremendously appreciated. The authors acknowledge the use of and the help of staff at the Cornell Nanobiotechnology Center and the Cornell Center for Materials Research (NSF award number DMR-1120296), specifically, Teresa Porri, Penny Burke, John Grazul, Mick Thomas, and John Hunt, for their assistance in using the tools and instruments in the Center, as well as for general upkeep of the facilities.

REFERENCES

- Donlan RM, Costerton JW. 2002. Biofilms: survival mechanisms of clinically relevant microorganisms. *Clin. Microbiol. Rev.* 15:167–193.
- Scallan E, Griffin PM, Angulo FJ, Tauxe RV, Hoekstra RM. 2011. Foodborne illness acquired in the United States—unspecified agents. *Emerg. Infect. Dis.* 17:16–22.
- Chmielewski RAN, Frank JF. 2003. Biofilm formation and control in food processing facilities. *Compr. Rev. Food Sci. Food Saf.* 2:22–32.
- Mitik-Dineva N, Wang J, Stoddart PR, Crawford RJ, Ivanova EP. 2008. Nano-structured surfaces control bacterial attachment, 113–116. *Int. Conf. Nanosci. Nanotechnol. (ICONN) 2008*, Melbourne, Australia, 25 to 29 February 2008.
- Flint SHH, Brooks JDD, Bremer PJJ. 2000. Properties of the stainless steel substrate, influencing the adhesion of thermo-resistant streptococci. *J. Food Eng.* 43:235–242.
- Scheuerman T, Camper A, Hamilton M. 1998. Effects of substratum topography on bacterial adhesion. *J. Colloid Interface Sci.* 208:23–33.
- Verran J, Rowe DL, Boyd RD. 2001. The effect of nanometer dimension topographical features on the hygienic status of stainless steel. *J. Food Prot.* 64:1183–1187.
- Boyd RD, Verran J, Jones MV, Bhakoo M. 2002. Use of the atomic force microscope to determine the effect of substratum surface topography on bacterial adhesion. *Langmuir* 18:2343–2346.
- Whitehead KA, Colligon J, Verran J. 2005. Retention of microbial cells in substratum surface features of micrometer and sub-micrometer dimensions. *Colloids Surf. B Biointerfaces* 41:129–138.
- Woodling SE, Moraru CI. 2005. Influence of surface topography on the effectiveness of pulsed light treatment for the inactivation of *Listeria innocua* on stainless-steel surfaces. *J. Food Sci.* 70:m345–m351.
- Dalby MJ, Riehle MO, Yarwood SJ, Wilkinson CD, Curtis AS. 2003. Nucleus alignment and cell signaling in fibroblasts: response to a micro-grooved topography. *Exp. Cell Res.* 284:272–280.
- Balasundaram G, Webster TJ. 2006. A perspective on nanophase materials for orthopedic implant applications. *J. Mater. Chem.* 16:3737–3745.
- Popat KC, Chatvanichkul K-I, Barnes GL, Latempa TJ, Jr, Grimes CA, Desai TA. 2006. Osteogenic differentiation of marrow stromal cells cultured on nanoporous alumina surfaces. *J. Biomed. Mater. Res. A.* 80A:955–964.
- Nikkhah M, Edalat F, Manoucheri S, Khademhosseini A. 2012. Engineering microscale topographies to control the cell-substrate interface. 2012. *Biomaterials* 33:5230–5246.
- Park MR, Banks MK, Applegate B, Webster TJ. 2008. Influence of nanophase titania topography on bacterial attachment and metabolism. *Int. J. Nanomed.* 3:497–504.
- Mitik-Dineva N, Wang J, Truong VKK, Stoddart PRR, Malherbe F, Crawford RJ, Ivanova EPP. 2009. Differences in colonisation of five marine bacteria on two types of glass surfaces. *Biofouling* 25:621–631.
- Díaz C, Schilardi PL, dos Santos Claro PC, Salvarezza RC, Fernandez Lorenzo De Mele MA. 2009. Submicron trenches reduce the *Pseudomonas fluorescens* colonization rate on solid surfaces. *ACS Appl. Mater. Interfaces* 1:136–143.
- Puckett SD, Taylor E, Raimondo T, Webster TJ. 2010. The relationship

- between the nanostructure of titanium surfaces and bacterial attachment. *Biomaterials* 31:706–713.
19. Cookson AL, Cooley WA, Woodward MJ. 2002. The role of type 1 and curli fimbriae of Shiga toxin-producing *Escherichia coli* in adherence to abiotic surfaces. *Int. J. Med. Microbiol.* 292:195–205.
 20. Prachaiyo P, McLandsborough L. 2000. A microscopic method to visualize *Escherichia coli* interaction with beef muscle. *J. Food Prot.* 63:427–433.
 21. Grivet M, Morrier JJ, Benay G, Barsotti O. 2000. Effect of hydrophobicity on in vitro streptococcal adhesion to dental alloys. *J. Mater. Sci. Mater. Med.* 11:637–642.
 22. Goldberg S, Davis JA, Hem JD. 1996. The surface chemistry of aluminum oxides and hydroxides, p 272–331. In Sposito G (ed), *The environmental chemistry of aluminum*, 2nd ed. CRC Press, Boca Raton, FL.
 23. Goloub TP, Koopal LK, Bijsterbosch BH, Sidorova MP. 1996. Adsorption of cationic surfactants on silica. Surface charge effects. *Langmuir* 12:3188–3194.
 24. Díaz C, Cortizo M, Schilardi P, Gomez de Saravia S, Fernández Lorenzo de Mele MA. 2007. Influence of the nano-micro structure of the surface on bacterial adhesion. *Mater. Res.* 10:11–14.
 25. Hochbaum AI, Aizenberg J. 2010. Bacteria pattern spontaneously on periodic nanostructure arrays. *Nano Lett.* 10:3717–3721.
 26. Singh AV, Vyas V, Patil R, Sharma V, Scopelliti PE, Bongiorno G, Podestà A, Lenardi C, Gade WN, Milani P. 2011. Quantitative characterization of the influence of the nanoscale morphology of nanostructured surfaces on bacterial adhesion and biofilm formation. *PLoS One* 6:e25029. doi:10.1371/journal.pone.0025029.
 27. Rizzello L, Sorce B, Sabella S, Vecchio G, Galeone A, Brunetti V, Cingolani R, Pompa PP. 2011. Impact of nanoscale topography on genomics and proteomics of adherent bacteria. *ACS Nano* 5:1865–1876.
 28. Prigent-Combaret C, Prensier G, Thi T, Vidal O, Lejeune P, Dorel C. 2000. Developmental pathway for biofilm formation in curli-producing *Escherichia coli* strains: role of flagella, curli and colonic acid. *Environ. Microbiol* 2:450–464.
 29. Pratt LA, Kolter R. 1998. Genetic analysis of *Escherichia coli* biofilm formation: roles of flagella, motility, and chemotaxis and type I pili. *Mol. Microbiol.* 30:285–293.